

2nd Sandia Fracture Challenge Summit: Sandia California's Modeling Approach

Kyle N. Karlson, Jay W. Foulk, and Arthur A. Brown

Prepared by
Sandia National Laboratories
Albuquerque, New Mexico 87185 and Livermore, California 94550

Sandia National Laboratories is a multi-program laboratory managed and operated by Sandia Corporation, a wholly owned subsidiary of Lockheed Martin Corporation, for the U.S. Department of Energy's National Nuclear Security Administration under contract DE-AC04-94AL85000.

Approved for public release; further dissemination unlimited.

Approach: Team Sandia California (Team H) used the Sandia code SIERRA Solid Mechanics: Implicit (SIERRA SM) to model the SFC2 challenge problem. SIERRA SM is a Lagrangian, three-dimensional, implicit code for the analysis of solids and structures. It contains a versatile library of continuum and structural elements, and an extensive library of material models. For all SFC2 related simulations, our team used Q1P0, 8 node hexahedral elements with element side lengths on the order 0.175 mm in failure regions. To model crack initiation and failure, element death removed elements from the simulation according to a continuum damage model. SIERRA SM's implicit dynamics, implemented with an HHT time integration scheme for numerical damping [1], was used to model the unstable failure modes of the models. We chose SIERRA SM's isotropic Elasto Viscoplastic material model for our simulations because it contains most of the physics required to accurately model the SFC2 challenge problem such as the flexibility to include temperature and rate dependence for a material. However, since the Elasto Viscoplastic model does not support anisotropic plastic behavior, the anisotropy evident in the provided data was included through other means described in detail in the following section.

The Elasto Viscoplastic plasticity model is an internal state variable model for describing the finite deformation behavior of metals. It uses a multiplicative decomposition of the deformation gradient into elastic, plastic, and isotropic damage and thermal expansion parts. The model considers the natural configuration defined by this decomposition and its associated thermodynamics. The model incorporates strain rate and temperature sensitivity, as well as damage, and tracks history dependence through the use of internal state variables. In its full form, the model has considerable complexity, but most of the material parameters and resulting behavior are optional with the exception of two elastic constants and a yield strength. Specifying only these three parameters would result in an elastic, perfectly-plastic material model.

The form of the material model specific to our use for SFC2 will now be outlined for the simplified case of uniaxial tension. For this simplified case, the stress evolves according to

$$\dot{\sigma} = E (\dot{\epsilon} - \dot{\epsilon}_p) \quad (1)$$

where ϵ is the total strain and ϵ_p is the plastic strain. The flow rule is defined by

$$\dot{\epsilon}_p = f \sinh^n \left(\frac{\sigma_y - \kappa}{Y} - 1 \right) \quad (2)$$

where σ_y is the equivalent stress; Y is a material parameter representing the rate independent, initial yield stress; f and n are material parameters that govern the material rate dependence; and κ is the isotropic hardening variable for the material, which evolves according to a hardening minus dynamic recovery model originally proposed by Kocks and Mecking [2]:

$$\dot{\kappa} = \kappa \frac{\dot{\mu}}{\mu} + (H - R_d \kappa) \dot{\epsilon}_p. \quad (3)$$

The temperature dependence for all material parameters (Y , f , n , H , R_d) can be specified explicitly with user specified scaling functions or using functional forms built into the model. Heat generation due to plastic work is calculated with

$$\dot{q} = \beta \sigma \dot{\epsilon}_p \quad (4)$$

where the material parameter β is the fraction of plastic work dissipated as heat.

The Elasto Viscoplastic model contains a void growth model and a void nucleation model to account for isotropic material damage. For void growth, damage evolves according to the model proposed by Cocks and Ashby [3]:

$$\dot{\phi} = \sqrt{\frac{2}{3}} \dot{\epsilon}_p \frac{1-(1-\phi)^{m+1}}{(1-\phi)^m} \sinh \left[\frac{2(2m-1)}{2m+1} \frac{p}{\sigma_{vm}} \right] \quad (5)$$

where σ_{vm} is the von Mises stress, p is the hydrostatic stress, ϕ is the void volume fraction of the material and the damage exponent m is a material parameter. With this void growth model, damage will only increase when $p/\sigma_{vm} > 0$. To account for damage resulting from other stress states, the void nucleation model based on work by Horstemeyer and Gokhale [4] is also included in the Elasto Viscoplastic material model:

$$\dot{\eta} = \eta \dot{\epsilon}_p \left\{ N_1 \left[\frac{4}{27} - \frac{J_3^2}{J_2^3} \right] + N_2 \frac{J_3}{J_2^{3/2}} + N_3 \left\| \frac{I_1}{\sqrt{J_2}} \right\| \right\} N_4 \quad (6)$$

where N_i are material parameters, η is the number of nucleated voids, and I_i and J_i are the stress invariants and deviatoric stress invariants, respectively. These two damage models can be used independently or concurrently to model damage in the material. Including damage evolution through these models reduces the material's elastic modulus and shear modulus by a factor of $1 - \phi$, and the flow rule becomes

$$\dot{\epsilon}_p = f \sinh^n \left[\frac{\sigma_y - \kappa(1 - \phi)}{Y(1 - \phi)} - 1 \right]. \quad (7)$$

The damage models require the definition of the initial void volume fraction ϕ_0 , the initial size of nucleated voids ϕ_0^η , and the initial void count per volume η_0 . To avoid numerical issues due to heavily distorted elements, a void coalescence damage ϕ_{coal} can be specified such that any elements with $\phi = \phi_{coal}$ at any of its integration points will be removed from the model through element death.

Material Parameter Calibration: We populated the Elasto Viscoplastic material parameters for Ti-6Al-4V sheet using a combination of the data provided in the challenge announcements and data from literature. Initially, the yield (Y , f , and n) and hardening (H and R_d) parameters were calibrated to the provided tensile data using a non-linear, least squares algorithm where the objective function consisted of the error between the provided data and the results from a model of the tension specimen. Since the rate dependence for the initial yield stress is not uniquely constrained by two data points, we used rate dependence data from Follansbee and Gray to supplement the data at two rates provided for the challenge. Temperature dependence was added to the initial yield stress Y and the elastic material properties according to data available in MMPDS-08 [5] and we used literature sources to inform our choice of β . Accurately modeling the temperature rise in the calibration specimens and resulting softening required a coupled thermo-mechanical simulation with thermal expansion, specific heat, thermal conductivity and emissivity determined from MMPDS-08. Void growth damage parameters were chosen based on prior experience with the material model and a sensitivity study of the model to the damage exponent m . Figure 1 contains the tension simulation results for the initial calibrated parameter set and the values for this parameter set.

After calibrating the model to the tension data, the shear data was incorporated into the model. Using the material parameter set calibrated to the tension data, a model of the shear test did not accurately predict the yield behavior of the specimen indicating that the material exhibits an anisotropic yield surface. By reducing the initial yield parameter Y by $\sim 83\%$, the shear simulation results improved and compared well to the test data.

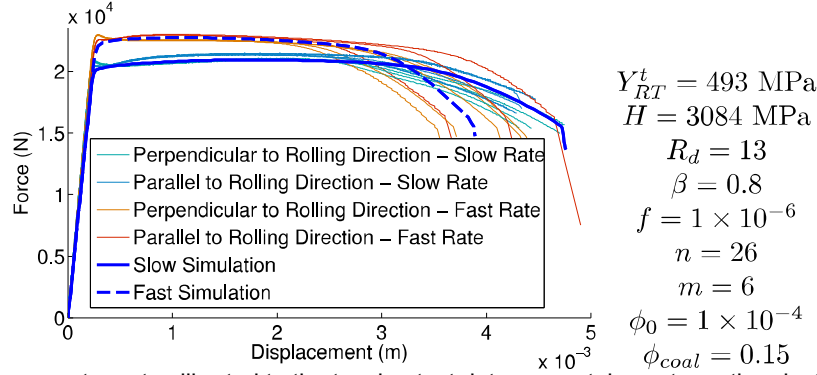


Figure 1. The parameter set calibrated to the tension test data accurately captures the plasticity and failure behavior of the data.

Since damage cannot evolve in pure shear with the void growth model alone, sensitivity studies performed on the void nucleation material parameters lead to the selection of the appropriate N_i , ϕ_0^η and η_0 parameters to capture shear failure. Figure 2 contains the calibrated shear simulation results and the values of the corresponding parameter set.

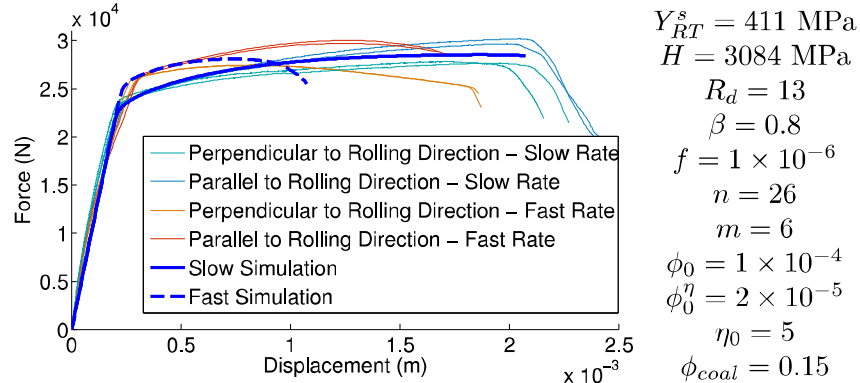
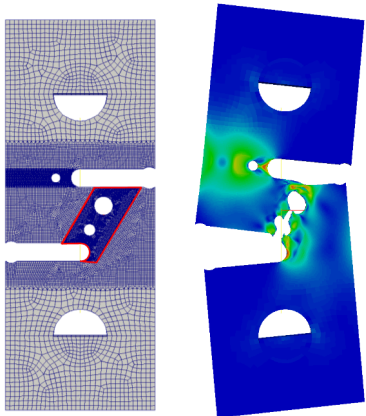


Figure 2. A separate parameter set with lower yield and void nucleation parameters accurately models the yield behavior of the shear test for both rates and failure for the slow rate.

Challenge Specimen Modeling Details: Model development for the challenge specimen included specifying the appropriate boundary conditions and incorporating anisotropy. The solid mechanics boundary conditions consisted of a symmetry boundary condition along the half-thickness plane of the specimen and approximations of the pin boundary conditions in the test. A half pin contiguously meshed into the specimen with the center node line having prescribed displacements approximated frictionless pins. The top pin's centerline was fixed and the bottom pin's centerline was displaced downward with a rate corresponding to the test rates. As stated previously, accurately modeling the calibration specimens required a coupled thermo-mechanical simulation. The thermal boundary conditions included radiation from the specimen surface to the room temperature surroundings and a symmetry boundary condition along the half-thickness plane of the specimen. Since the Elasto Viscoplastic model cannot accommodate an anisotropic yield surface, the model of the specimen was split into two element blocks: Block 1 with a yield corresponding to the tension initial yield Y_{RT}^t and Block 2 with a lower yield $Y_{RT}^{S*} = 441$ MPa since that region is initially predominantly in shear. **Figure 3** depicts Block 2 outlined in red with the remaining elements belonging to Block 1. Since the stress state in Block 2 does not directly correspond to that of failure region in the shear model, a simulation of the challenge specimen at the slow rate using a rate and temperature independent Hill plasticity model influenced the selection of

$Y_{RT}^{S*} = 441$ MPa. All simulations consisted of models constructed at the nominal dimensions according to the specimen drawings.



Blind Predictions: Using the material model parameters and boundary conditions specified in the previous sections, the challenge specimen model predicted failure through crack path B-D-E-A for both rates. For both rates, the crack propagated unstably through B-D-E, as shown in Figure 3, while the remaining ligament carried load until tensile failure occurred much further into the simulation (~375 seconds for the slow rate and ~.36 seconds for the fast rate). Table 1 lists the maximum loads and CODs at crack initiation for each rate and Figure 4 displays the predicted load versus COD1 plot for both rates.

Figure 3. On the left, Block 2 is outlined in red on the undeformed model geometry. On the right, the deformed geometry is shown after the crack has propagated into the upper hole in an unstable manner.

Displacement Rate (mm/s)	Peak Load (N)	COD1 @ Crack Initiation (mm)	COD2 @ Crack Initiation (mm)
25.4	20,310	2.966	2.644
0.0254	20,244	4.359	3.451

Sources of Error: Several sources of error were present in the challenge specimen

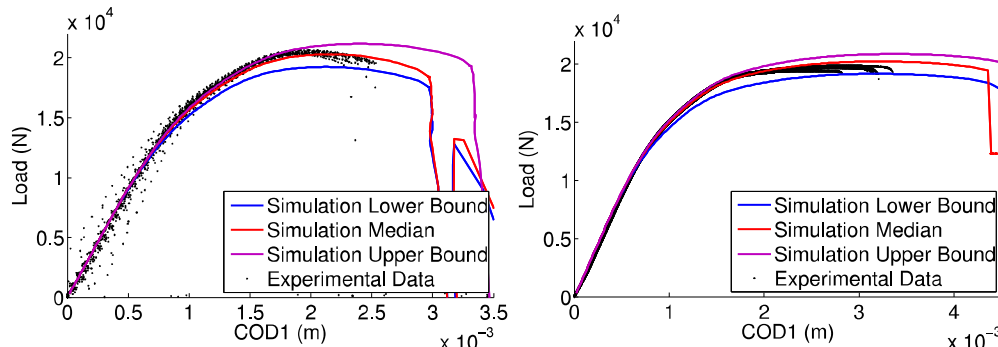


Figure 4. The load versus COD1 predictions for fast rate (left) and the slow rate (right) correspond to the experimental data; however, both models over predicted COD1 at crack initiation.

model. For example, an isotropic material model was used to simulate the anisotropic material through the use of separate element blocks and material parameters. Ideally, an anisotropic material model with rate and temperature dependence similar to Elasto Viscoplastic would have been used. Additionally, material parameter uncertainties were large and sensitivity studies show these uncertain parameters had significant effects on the simulation results. Numerical modeling issues also introduced error. SIERRA SM's implicit contact algorithm would not converge causing the implementation of the frictionless pin for the model. Also, mesh dependent failure models in SIERRA SM are not fully developed; therefore, rigorous mesh convergence studies could not be performed and the submitted predictions may not be the converged solution.

References

- [1] H. M. Hilber, T. J. R. Hughes, and R. L. Taylor, "Improved Numerical Dissipation for Time Integration Algorithms in Structural Dynamics," *Earthquake Engineering and Structural Dynamics*, vol. 5, no. 3, pp. 283-292, 1977.
- [2] U. F. Kocks and H Mecking, "A mechanism for static and dynamic recovery," *Strength of Metals and Alloys*, pp. 345-350, 1979.
- [3] A. Cocks and M. Ashby, "Intergranular fracture during power-law cree under multiaxial stresses," *Metal Science*, vol. 14, no. 8-9, pp. 395-402, August 1980.
- [4] Mark F. Horstemeyer and Arun M. Gokhale, "A void-crack nucleation model for ductile metals," *Internation Journal of Solids and Structures*, vol. 36, no. 33, pp. 5029-5055, November 1999.
- [5] Federal Aviation Administration, *Metallic Materials Properties Development and Standardization*. Washington, D.C.: Battelle Memorial Institute, 2013.